RSC Advances

PAPER

View Article Online
View Journal | View Issue

Cite this: *RSC Adv.*, 2023, **13**, 21336

Highly sensitive capacitance-based nitrite sensing using polydopamine/AuNPs-modified screen-printed carbon electrode†

Faisal K. Algethami, *[a] Amal Rabti, [bc] Mohamed Mastouri, [b] Babiker Y. Abdulkhair, [a] Sami Ben Aoun [d] and Noureddine Raouafi *[b]

Received 11th June 2023
Accepted 10th July 2023

DOI: 10.1039/d3ra03898j

rsc.li/rsc-advances

Regulatory bodies play a crucial role in establishing limits for food additives to ensure food quality and safety of food products, as excessive usage poses risks to consumers. In the context of processed animal-based foodstuffs, nitrite is commonly utilized as a means to slow down bacterial degradation. In this study, we have successfully leveraged the redox activity of an electrochemically deposited polydopamine (pDA) film onto gold nanoparticle (AuNP)-modified screen-printed electrodes (SPCE) to develop a sensitive and versatile methodology for the detection of nitrite using redox capacitance spectroscopy. By exploiting the interaction of the AuNPs/pDA electroactive interface with the target nitrite ions, we observed distinct changes in the redox distribution, subsequently leading to modifications in the associated redox capacitance. This alteration enables the successful detection of nitrite, exhibiting a linear response within the concentration range of 10 to 500 μM, with a limit of detection of 1.98 μM (S/N = 3). Furthermore, we applied the developed sensor to analyze nitrite levels in processed meats, yielding good recoveries. These results demonstrate the potential of our approach as a promising method for routine detection of ions.

1 Introduction

Nitrite salts, such as potassium nitrite (KNO_2, E249) and sodium nitrite ($NaNO_2$, E250), are commonly used as food additives to preserve processed animal-based products, vegetables and other foodstuffs.[1,2] Nitrite ions play a critical role in inhibiting the growth of harmful bacteria and preventing spoilage in meat. By acting as an antimicrobial agent, nitrite extends the shelf life of processed meats ensuring their safety for consumption.

However, the use of nitrite in food preservation is not without concerns.[3,4] One significant issue is the potential formation of nitrosamines when nitrite reacts with naturally occurring amines present in meat. Nitrosamines are known to be carcinogenic and have been linked to an increased risk of cancer.[5,6] Therefore, regulatory bodies carefully monitor and impose limits on the allowable levels of nitrite in processed meats aiming to mitigate these risks and protect consumer health. Indeed, the maximum residue levels (MRLs) vary from 50 to 150 mg kg^{-1}, which is *ca.* 1 to 3 μM in processed meat and cheese.[3]

Numerous analytical techniques have been developed for the detection of nitrite, including chemiluminescence,[7] fluorescence,[8,9] nanoplasmonic colorimetry,[10] Raman spectroscopy[11] and electrochemistry.[12–14] Among these methods, electrochemical detection stands out due to its higher sensitivity, lower cost and adaptability to various applications, making it suitable for widespread use. Nevertheless, direct oxidation of nitrite at conventional electrodes poses a challenge due to its high overpotential.[15] To overcome this challenge, surface modification of electrode becomes necessary. Various nanomaterials such as noble metals[16] or carbonaceous[17] nanomaterials, organic conducting polymers[14] and 2D MXenes[18] are commonly used to functionalize the electrode surface. While techniques like cyclic voltammetry (CV), differential pulse voltammetry (DPV) and square wave voltammetry (SWV), or amperometry and electrochemical impedance spectroscopy (EIS) are commonly used in the sensor design, electrochemical capacitance spectroscopy (ECS) or impedance-derived capacitance approach is considered as an interesting alternative. ECS offers improved signal sensitivity and lower detection limits in chemical[19,20] and biochemical[21–23] sensing applications. In ECS, the measured signal, known as redox capacitance, is a feature of electroactive nanoscale films relies solely on changes in the electrostatic environment of electroactive groups. For effective capacitance

[a]*Department of Chemistry, College of Science, Imam Mohammad Ibn Saud Islamic University (IMSIU), P.O. Box 90950, Riyadh 11623, Saudi Arabia. E-mail: noureddine.raouafi@fst.utm.tn falgethami@imamu.edu.sa*

[b]*Sensors and Biosensors Group, Analytical Chemistry and Electrochemistry Lab (LR99ES15), Department of Chemistry, Faculty of Science, University of Tunis El Manar, Tunis El Manar, 2092 Tunis, Tunisia*

[c]*National Institute of Research and Physicochemical Analysis (INRAP), Laboratory of Materials, Treatment, and Analysis (LMTA), Biotechpole Sidi Thabet, 2020 Sidi Thabet, Tunisia*

[d]*Department of Chemistry, Faculty of Science, Taibah University, P.O. Box 30002, Al-Madinah Al-Munawwarah, Saudi Arabia*

† Electronic supplementary information (ESI) available. See DOI: https://doi.org/10.1039/d3ra03898j

assays, nanoscale redox-active structures need to be tethered onto electrode surfaces.[21] To achieve this, various ferrocene composites and derivatives such as self-assembled 11-ferrocenylundecanethiol,[24] ferrocene-modified silicon nanoparticles,[20] ferrocene-tagged peptides,[21,25] tetraethylene glycol ferrocene derivative[26] and aptamer-modified magnetic beads bearing ferrocene[23] have been employed. Furthermore, MoS_2 nanosheets,[27] Prussian Blue nanostructured films[28] and electrochemically deposited polycatechol[22] have served successfully as redox capacitance transducers. Among these options, conductive polydopamine films exhibit interesting properties, including their favourable adhesion, the presence of electroactive sites able to attach biomolecules and rapid electron transfer rates. These qualities enable a rapid interface with various electrochemical signals, making conductive polydopamine films suitable for designing unique diagnostic tools.[29]

In this study, we introduced a novel approach for the detection of nitrite ions in processed meat samples. The methodology involved the electrochemical deposition of a conductive polydopamine (pDA) film onto a screen-printed carbon electrode that was previously modified with gold nanoparticles. The use of gold nanoparticles was justified by their advantageous properties, including a large surface area, high electrical conductivity and excellent catalytic activities.[30] The redox activity of pDA and its known interaction with nitrite[31,32] made it a suitable candidate for transducing the nitrite ions detection event. Notably, while the combination of AuNPs and pDA for sensing purposes has been described previously,[33,34] the focus has mainly been on exploiting the direct electrochemistry of the analyte or utilizing external labels to transduce the sensing event. In contrast, our study demonstrated the application of the redox activity of the pDA film itself for label-free detection of nitrite ions.

To evaluate the levels of nitrite, we measured the variation in pDA redox capacitance using electrochemical impedance spectroscopy (EIS)-derived electrochemical capacitance spectroscopy. The developed sensor exhibited good sensitivity and selectivity for nitrite determination, showcasing its potential as a reliable detection method. Importantly, the sensor successfully detected nitrite in processed meat samples, demonstrating its applicability in real-world scenarios. The innovative combination of a conductive polydopamine film, gold nanoparticles and EIS-based capacitance measurements offers a promising approach for the sensitive and selective detection of nitrite, particularly in processed meat products.

The findings of this study make notable contributions to the field of food safety analysis and hold potential implications for quality control in the food industry. The sensor principle is depicted in Scheme 1.

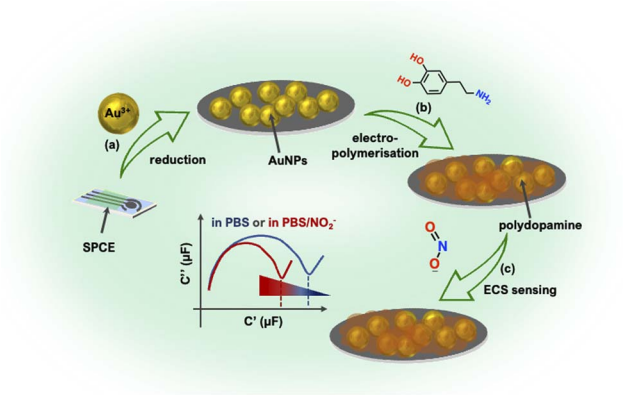

Scheme 1 Principle of the preparation and work of pDA/AuNPs/SPCE sensor for ECS sensing of nitrite.

2 Materials and methods

2.1 Chemicals

Tetrachloroauric acid trihydrate ($HAuCl_4 \cdot 3H_2O$, 99.9%), dopamine hydrochloride (98%), $NaNO_2$ (97%), H_2SO_4 (95%), HCl (37%), NaCl (99%), KCl (99%), NaH_2PO_4 (99%), K_2HPO_4 (99%), $K_4Fe(CN)_6 \cdot 3H_2O$ (99%) and $K_3Fe(CN)_6$ (99%) were purchased from Sigma-Aldrich (Germany) and used as received. Phosphate-buffered saline solutions (PBS, 10 mM) were prepared by dissolving NaCl, KCl, Na_2HPO_4 and KH_2PO_4 in deionized water (>18.2 MΩ cm).

All stock solutions were prepared by dissolving the desired amount of the chemical in PBS 10 mM solution unless otherwise specified.

2.2. Apparatus and electrodes

A Metrohm PGSTAT M204 potentiostat fitted with a FRA32 frequency response analyser for impedance, controlled by Nova® software (v2.1.6), was used to record all electrochemical measurements. Screen-printed carbon electrodes (SPCE, OHT-000), where carbon material is used to make the working (4 mm diameter) and counter electrodes and the pseudo-reference electrode is a silver-based electrode, were purchased from Orion Hi-Tech S.L. (Madrid, Spain).

2.3. Sensor preparation

2.3.1. Electrodeposition of gold nanoparticles. SPCEs were modified according to a previous report.[35] Briefly, the electrodes were first cleaned using a PBS solution by sweeping the potential for 10 cycles from −0.5 to +1.0 V with a scan rate of 50 mV s^{-1}. Then, 50 μL of 1.0 mM $HAuCl_4$ dissolved in 10 mL HCl solution were dropped onto the electrode surface, a cathodic current ($i = -100$ μA) and a potential ($E_{app.} = +0.1$ V) were respectively applied for 240 and 120 seconds. The nanostructured electrodes were rinsed with deionized water and dried at room temperature (RT). Before the electrodeposition of the pDA film, the nanostructured electrodes were activated using a sulfuric acid solution (0.5 M) to remove the gold oxide layer by sweeping the potential from 0.0 to +1.5 V for 15 cycles at a scan rate of 100 mV s^{-1}. The fabricated AuNPs/SPCEs were electrochemically characterized by cyclic voltammetry in 0.5 M H_2SO_4 (Fig. S1 see ESI†).

2.3.2. Polydopamine deposition. The pDA film was deposited onto AuNPs/SPCEs using a potential pulse sequence of 0.5 V for 2.0 s, 0.0 V for 2.0 s,-0.3 V for 2 s and 0.0 V for 3.0 s with 30 applied pulse cycles.[36] The deposition was made in a freshly prepared 1.0 mg L^{-1} concentration of dopamine hydrochloride dissolved in 10 mM PBS buffer (pH 7.0).

To examine the preparation protocol reproducibility, five different electrodes were prepared, and their electrochemical behaviours were compared.

2.4. Electrochemical measurements

CV and EIS were used to follow the stepwise modification of the SPCE surface. The EIS diagrams were recorded in a PBS solution containing 5 mM concentrations of $K_3Fe(CN)_6/K_4Fe(CN)_6$ (1 : 1) as a redox probe. The frequency was swept from 0.01 Hz to 10 kHz by applying a constant potential of 0.180 V *vs.* Ag/AgCl and with an amplitude modulation of 0.20 V. Randles' equivalent circuit $[R_s(C[R_{ct}W])]$; where, R_s: the solution resistance; C: the capacitance; R_{ct}: the charge-transfer resistance and W: the Warburg impedance; was used to fit the Nyquist plots.

For the detection of nitrite, EIS measurements were carried out, in triplicate, in PBS 10 mM solution with a frequency ranging from 100 kHz to 0.1 Hz at an applied potential of 0.14 V (half-wave potential of pDA film) *vs.* Ag/AgCl and with an amplitude modulation of 0.20 V. The raw complex EIS data represented by $Z^*(\omega)$ were converted to complex capacitance data $C^*(\omega)$ using the eqn (1) and (2):

$$C' = -Z''/\omega|Z|^2 \quad (1)$$

$$C'' = Z'/\omega|Z|^2 \quad (2)$$

where C' and C'' are respectively the real and imaginary capacitance components, ω is the angular frequency and $|Z|$ is the modulus of Z^*.[37] Subsequently, redox capacitance "C_r" values were extracted graphically by fitting the obtained semicircles using Origin 8.0 software and the relative response (% RR) is calculated using eqn (3).

$$\%\ \mathrm{RR} = 100 \times \frac{C_r^{-1} - C_{blank}^{-1}}{C_{blank}^{-1}} \quad (3)$$

where C_r and C_{blank} are the capacitance values of the sensor in presence and absence of nitrite, respectively.

The reproducibility of the sensor was assessed by registering the % RR value of five electrodes prepared separately in presence of 1 mM $NaNO_2$.

2.5. Nitrite extraction from processed meat samples

10 g of processed meat (salami and ham purchased from a local market) were blended using a kitchen blender for 30 seconds, then 30 mL of deionized water were added. The mixture was ultrasonicated for 30 minutes at 30 °C and left to settle down for 10 minutes before being filtered using a 0.45 μm membrane. Then, the filtrate was heated at 70 °C for 45 minutes. Afterwards, the filtrated sample were diluted 10 times with a PBS solution before being doped with different concentrations (10, 25 and 50 μM) of nitrite solution.

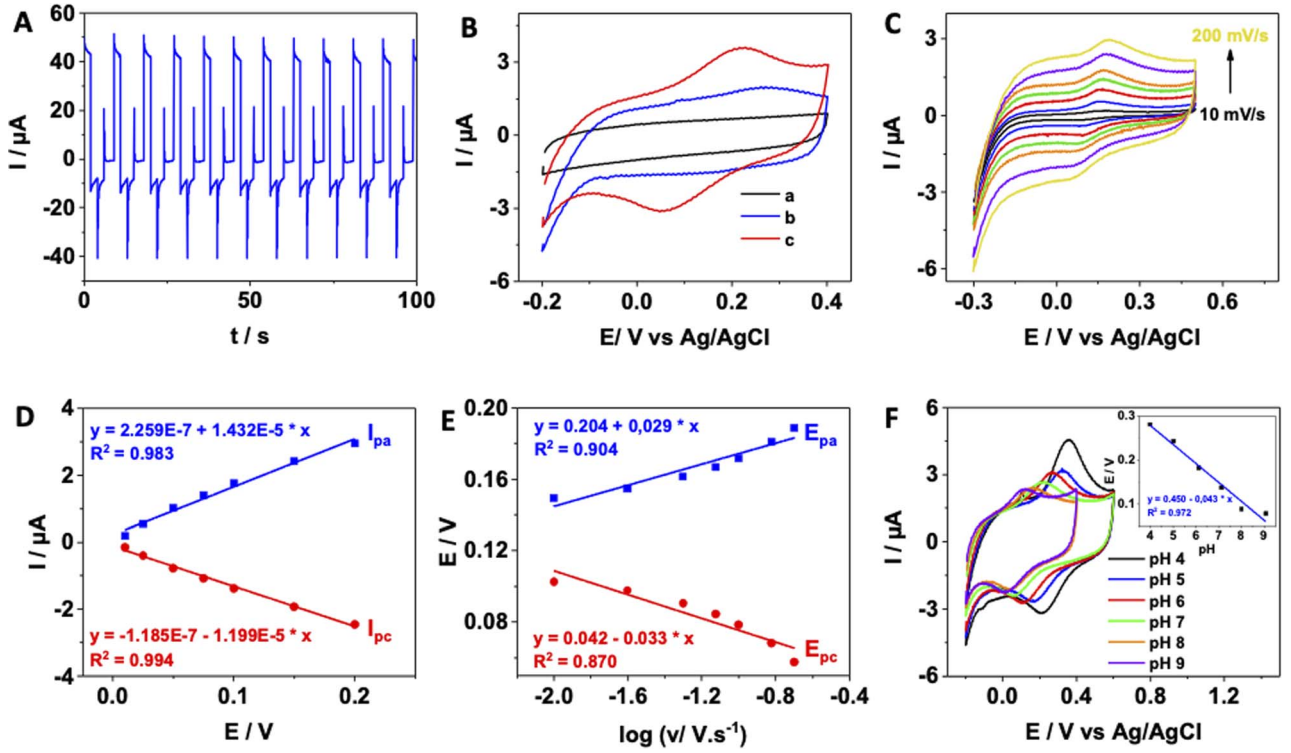

Fig. 1 (A) Electrochemical deposition and characteristics of the polydopamine film. *I*–*t* curve of first 100 s of the pulse deposition (30 pulse cycles) of 1 mg mL^{-1} of dopamine in 10 mM PBS (pH 7.0) at AuNPs/SPCE. (B) CV of SPCE (a), AuNPs/SPCE (b) and pDA/AuNPs/SPCE (c) in 0.01 M PBS (pH 7.0) at 100 mV s^{-1}. (C) CVs of pDA/AuNPs/SPCE in 0.01 M PBS (pH 7.0) at different scan rates (from inner to outer: 10–200 mV s^{-1}); (D) plots of anodic and cathodic peak currents *vs.* scan rate of pDA/AuNPs/SPCE in 0.01 M PBS (pH 7.0). (E) Plots of peak potentials *vs.* logarithm of the scan rate for the pDA/AuNPs/SPCE in 0.01 M PBS (pH 7.0). (F) CVs of PDA/AuNPs/SPCE in 0.01 M PBS at different pH (inset: plot of the formal potential *vs.* pH value).

3. Results and discussion

3.1. Electrochemical behaviour of the pDA/AuNPs/SPCE

3.1.1. pDA deposition. The electrochemical deposition of polydopamine (pDA) on conductive substrates can be achieved through cyclic voltammetry[38,39] or pulsed deposition,[40,41] both of which are fast-coating processes that offer excellent control over film thickness. While pDA film growth *via* auto-oxidation or dip-coating typically takes several hours, electrochemically deposited pDA films can be obtained with reproducible thickness and morphology within a few minutes. It is worth noting that pulse deposition process as compared to cyclic voltammetry, leads to the formation of denser and more cross-linked films.[41] In this study, the latter method was used to form an electrochemically deposited pDA film on AuNPs/SPCE surfaces as shown in Fig. 1A.

To investigate the characteristics of the modified electrode surface, cyclic voltammetry measurements were performed on SPCE, AuNPs/SPCE and pDA/AuNPs/SPCE in the potential range of −0.2 to 0.4 V in 0.01 M PBS (pH 7.0) as depicted in Fig. 1B. While SPCE and AuNPs/SPCE exhibited no electrochemical activity, the cyclic voltammogram of pDA/AuNPs/SPCE displayed a pair of oxidation and reduction peaks at ∼0.08 and ∼0.20 V *vs.* Ag/AgCl, respectively. The peak-to-peak separation is equal to 120 mV and an ip_c-to-ip_a ratio is close to unity suggesting a quasi-reversible electron transfer process. These observed peaks, attributed to the oxidation and reduction of catechol and quinone units present in pDA film,[42] clearly indicate the successful electrodeposition of pDA onto the AuNPs/SPCE surface.

3.1.2. Effects of scan rate. The cyclic voltammetry curves of the pDA-modified AuNPs/SPCE were recorded in PBS (pH 7.0) at various scan rates as depicted in Fig. 1C. Both the anodic and cathodic peak currents exhibited linear increase with scan rates ranging 10 and 200 mV s^{-1} (Fig. 1D), indicating a surface confined redox process.[42] By analyzing the slope of the peak currents plotted against the scan rate, the surface coverage (Γ) of the pDA film on the electrode surface was estimated using eqn (4):[43,44]

$$I_p = n^2F^2vA\Gamma/4RT \quad (4)$$

In eqn (4), F represents the Faraday constant (96 485 C mol^{-1}), v is the scan rate (V s^{-1}); A denotes the effective area (cm^2) calculated in ESI,† R represents the gas constant (8.314 J K^{-1} mol^{-1}) and T is the room temperature (298 K). Assuming a number of electrons transferred as 2, the surface coverage (Γ) was calculated to be 7.48 × 10^{-11} mol cm^{-2} which is comparable to that of 1.70 × 10^{-10} mol cm^{-2} at pDA@ERGO/GCE.[45] The difference is likely attributed to the superior electrocatalytic activity of graphene compared to AuNPs.

Fig. 1E illustrates that the anodic and cathodic peak potentials of the pDA film exhibited linear dependence on the logarithm of the scan rates within the range of 10–200 mV s^{-1}. By analyzing the slope of the E *vs.* log(v) plot, the electron-transfer coefficient (α) can be calculated using eqn (5):[46]

$$E_{pa} = [2.303 \times RT/(1 - \alpha)n\alpha F]\log(v) + K \quad (5)$$

where, $n\alpha$ represents the number of involved electrons in the rate-determining step, K is a constant and the remaining parameters are provided in eqn (4). Assuming that $n\alpha$ equals 2, α was estimated to be *ca.* 0.89. The obtained coefficient is in good agreement with the values of 0.80 and 0.75 obtained for pDA/SPCE[42] and for pDA@ERGO/GCE,[45] respectively.

3.1.3. pH-potential dependence. The oxidation–reduction peak potential of the pDA film is dependent on the pH of the solution. Both the anodic and cathodic peak potentials of the pDA-modified electrode shifted toward more negative with increasing solution pH as shown in Fig. 1F. The formal potential exhibited linear dependence on the pH values ranging from 4 to 9 with a slope of −43 mV pH^{-1} (inset of Fig. 1F). This value is close to the theoretical value of −58.6 mV pH^{-1}, indicating the involvement of two electrons and two protons in the electron transfer process.[39]

Furthermore, to assess the reproducibility of the preparation protocol, five different electrodes were prepared, and their electrochemical behaviours were compared. The results showed that the anodic peak current of the pDA film exhibited a relative standard deviation of approximately 8%, indicating a controllable electrode preparation.

3.1.4. EIS characterization. In order to investigate the stepwise electrode modification, electrochemical impedance spectroscopy measurements were carried out in 5 mM $[Fe(CN)_6]^{3-/4-}$ as the redox probe. Nyquist plots were fitted to the Randles' equivalent circuit model (Fig. 2A). Upon the introduction of gold nanoparticles onto the bare SPCE surface,

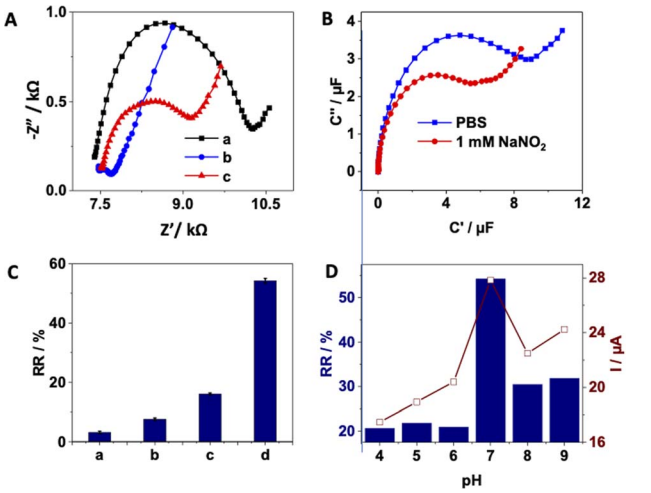

Fig. 2 Modified electrode characterization and dependence on the solution pH. (A) Nyquist plots in 5 mM equimolar concentrations of $K_3Fe(CN)_6/K_4Fe(CN)_6$ of (a) bare SPCE; (b) AuNPs/SPCE; and (c) pDA/AuNPs/SPCE. (B) Capacitance Nyquist plots of pDA/AuNPs/SPCE in the absence and presence of 1 mM $NaNO_2$ in 0.01 M PBS (pH 7.0). (C) The relative variation of redox capacitance % RR of (a) bare SPCE; (b) AuNPs/SPCE; (c) pDA/SPCE; and (d) pDA/AuNPs/SPCE after addition of 1 mM $NaNO_2$. Error bars, SD, $n = 3$. (D) The % RR and the current peak intensity of the CV voltammograms of pDA/AuNPs/SPCE registered in 1 mM $NaNO_2$ at different pH of PBS solution.

a significant decrease in the charge transfer resistance was observed ($R_{ct} = 2275.3 \pm 68.4\ \Omega$ for the bare SPCE and $240.6 \pm 27.8\ \Omega$ for AuNPs/SPCE). The successful electrodeposition of the pDA film was further confirmed by an increase in the charge transfer resistance ($R_{ct} = 1182.8 \pm 46.0\ \Omega$ for pDA/AuNPs/SPCE).

3.2. Capacitive detection of nitrite

For the capacitive detection of nitrite, the applied potential was fixed at 140 mV, corresponding to the half-wave potential of the redox pDA film. Fig. 2B illustrates the ECS spectra of pDA/AuNPs/SPCE before and after the addition of 1000 μM concentration of $NaNO_2$. It can be observed that the semicircle, associated with the complex capacitance data composed of faradaic and non-faradaic film contributions of the studied electrode,[47] decreased after the addition of nitrite. Similar behaviour was observed for AuNPs/SPCE (Fig. S2 in ESI†) and pDA/SPCE (Fig. S3 in ESI†), while the capacitance of SPCE remained almost unchanged (Fig. S4 in ESI†). However, when comparing the relative capacitance response (Fig. 2C), the highest value was observed for the pDA/AuNPs/SPCE. The decrease in capacitance after the addition of nitrite for the gold-nanostructured electrode is attributed to its good electrocatalytic properties.[30] In the case of pDA-modified electrodes, this behaviour is a result of the formation of hydrogen bonds between NO_2^- and pDA redox moieties, leading to a decrease in electronic density in the molecular receptive layer after the interaction with nitrite ions. Additionally, chemical reaction between nitrite and the reduced form of pDA can be expected. Previous studies by Lu *et al.* demonstrated rapid nitration and nitrosation of hydroquinone, catechol and resorcinol using HPLC/MS.[32] Furthermore, the large surface area and good conductivity of gold nanoparticles allow for a higher surface coverage of the pDA films, which explains the higher relative capacitance of pDA/AuNPs/SPCE compared to pDA/SPCE. These results correlated well with the data from cyclic voltammetry recorded in presence of nitrite (Fig. S5 in ESI†), where the highest peak current in the presence of nitrite was obtained on pDA/AuNPs/SPCE.

To maximize the electrode response towards nitrite, the response of pDA/AuNPs/SPCE was evaluated at different pH values ranging from 4 to 9. Fig. 2D shows an increase in the relative capacitance response as the pH increased to 7, followed by a decrease in % RR at higher pH values. This observed capacitance behaviour correlates well with the intensity of the nitrite peak current recorded by cyclic voltammetry (Fig. 2D and S6†). The lower % RR value in acidic solutions is attributed to the decomposition of nitrite to nitric oxide and nitrate,[48] while the decrease in % RR value in basic solutions is related to the insufficient protons necessary for the electrocatalytic oxidation of nitrite.[49] Therefore, a 0.01 M PBS (pH 7.0) buffer was used for the detection of nitrite.

3.3. Analytical performance

3.3.1. Linear range and detection limit. The linear range and detection limit of the developed sensor were evaluated, EIS and ECS spectra were recorded for various nitrite concentrations. Impedance measurements, specifically the charge-transfer resistance remained almost unchanged with increasing ion concentrations (Fig. 3A), while the derived capacitance signal decreased proportionally with increasing nitrite concentrations (Fig. 3B). The measured capacitance signal solely depends on the faradaic capacitive charging of the redox polydopamine film. As the pDA redox moiety gradually occupies lower electronic density in the molecular receptive layer, the capacitance signal decrease.[26] Additionally, hydrogen or chemical bonding between NO_2^- and the pDA redox moieties reduce the number of free PDA redox moieties, thereby decreasing their respective redox capacitance. Plotting the relative capacitance response against the logarithm of the nitrite concentrations resulted in a straight line ranging from 10 μM to 500 μM with a correlation coefficient (R^2) of 0.987 (Fig. 3C). The limits of detection (LOD, S/N = 3) and quantification (LOQ, S/N = 10) were estimated to be 1.98 μM and 6.53 μM, respectively.

The reproducibility of the sensor was assessed by measuring the % RR value of five separately prepared electrodes in the presence of 1 mM $NaNO_2$. The obtained relative standard deviation of 3.6% indicates a good electrode-to-electrode reproducibility thanks to the applied electrodeposition methods that allow highly reproducible preparation of both AuNPs and pDA layers. Moreover, the stability of the prepared sensor was evaluated by preparing two electrodes on the same day and measuring the % RR value in the presence of 1 mM $NaNO_2$ before and after four weeks of storage at 4 °C. The sensor retained approximately 95% of its initial % RR value, confirming a good stability.

3.3.2. Selectivity. To evaluate the practicality and selectivity of the developed sensor, several ions were added to the 0.01 M PBS (pH 7.0) solution containing 10 μM concentration of nitrite

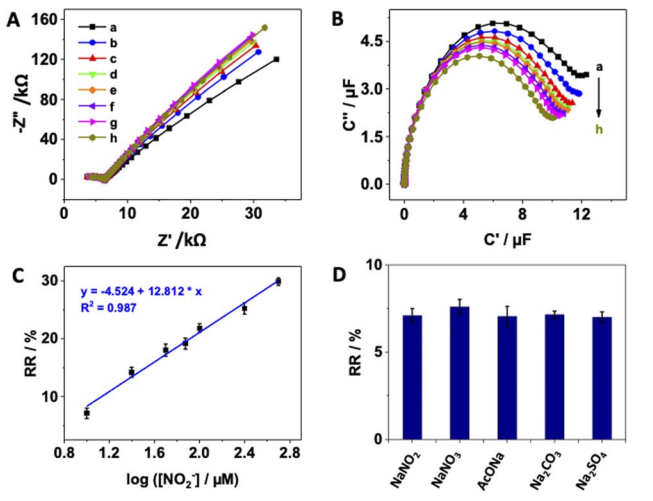

Fig. 3 Electrochemical performance determination of the pDA/AuNPs/SPCE. (A) EIS and (B) ECS Nyquist plots registered at various $NaNO_2$ concentrations: (a) 0 μM; (b) 10 μM; (c) 25 μM; (d) 50 μM; (e) 75 μM; (f) 100 μM; (g) 250 μM and (h) 500 μM. (C) Calibration curve of the developed sensor displaying the relative variation of redox capacitance % RR *vs.* log($[NO_2^-]$). (D) Histograms giving the relative variation of redox capacitance upon addition of 10 μM $NaNO_2$ with 1 mM of different interferents. Error bars, SD, $n = 3$.

ion. The results, shown in Fig. 3D, indicated that even at 100-fold concentrations of nitrate, acetate, carbonate and sulfate ions did not interfere with nitrite determination with a signal change of less than 4%. This suggests excellent selectivity of the method toward nitrite.

3.4. Comparison with literature

In comparison with previously reported gold nanomaterial based composite sensors for the detection of nitrite ions, the analytical performance of the prepared pDA/AuNPs/SPCE was found quite comparable, as summarized in Table 1. The linear range obtained in this study was larger than that of other sensors based on gold nanoparticles[50] or composites of gold nanoparticles with polymers,[51,52] AuPs-decorated CNTs,[53] or a mixture of polymers and carbon nanomaterials.[53–55] Additionally, the designed electrode exhibited a relatively lower detection limit than that of glassy carbon electrodes (GCE) modified with gold nanoparticles[56] or with a mixture of gold nanoparticles with graphene.[57]

While it is acknowledged that other amperometry- or voltammetry-based sensors for nitrite can achieve wider linear ranges and lower limits of detection, reaching nanomolar range, respectively,[16,58] the electrochemical impedance spectroscopy was used for the detection of aqueous anions such as carbonate, bicarbonate, chloride, acetate, sulfate[59] or perchlorate.[60] Redox capacitance spectroscopy was applied to quantitively detect perrhenate (ReO_4^-),[19] hydrogen sulfate, phosphate and chloride[61] ions. To the best of our knowledge, this study presents the first report of a capacitive-based sensor for nitrite with practical applications in real sample analysis, showing the impact of the sample matrix and provides effective strategies to overcome it. While it is worth mentioning the method exhibits a narrower dynamic range and lower limit of detection compared to several alternatives gathered in Table 1, its capabilities remain sufficient for accurately determining the levels of nitrite in processed meat. This is particularly relevant as the method closely aligns with the maximum residue limits (MRLs) established by food control agencies, which range from 1 to 3 μmol L^{-1}. On the other hand, the method is easy to implant since it uses low-effective screen-printed electrodes that can be modified with gold nanoparticles and dopamine-derived polymeric film, that can be achieved through an electrochemical deposition process in less 30 minutes.

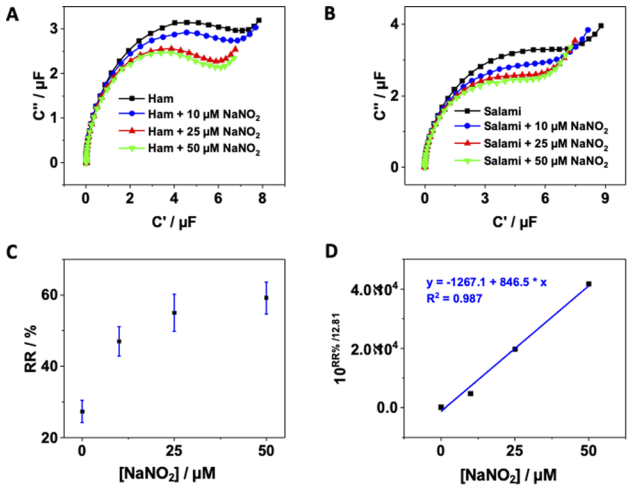

Fig. 4 ECS Nyquist plots registered in ham (A) and salami (B) samples spiked with various $NaNO_2$ concentrations. (C) Relative variation of redox capacitance *vs.* $\Delta[NO_2^-]$ in ham spiked samples. Error bars, SD, $n = 3$. (D) Graph of the proposed standard addition method application for nitrite determination in ham sample.

Table 1 Comparison of the prepared sensor performances with some of the gold nanomaterials-based composite as electrochemical sensing platforms for nitrite detection[a]

Electrode	Technique	LOD (μM)	Range (μM)	Ref.
AuNPs/CPE	SWV	0.2	0.2–15	50
AMPTS-AuNPs/GCE	*I–t*	1.0	1–12	51
AuNPs-PEI/GSPE	CV, DPV	1.0	1–10	52
AuNPs/f-MWCNT/LIG	SWV	0.9	10–140	53
GO-CS-AuNPs/GCE	*I–t*	0.3	0.9–18.9	54
Au–W bimetallic/GR-CS/PGE	CV	0.12	10–250	55
AuNPs/Gr/GCE	*I–t*	16.0	50–5100	57
AuNPs/GCE	CV	110.0	370–10 000	56
Au/PANI/CPE	*I–t*	25.0	38–1000	62
MoS_2-MWCNTs–Au/GCE	*I–t*	4.0	12–6500	63
Dy_2O_3-AuNPs/GCE	CV	3.3	0.01–1000	64
3D Au–rGO/FTO	CV	12.1	29.9–5740	65
AuNPs/MoS_2/GN/GCE	CV	1.0	5–5000	66
Au-$Dy_2(WO_4)_3$/GCE	DPV	3.5	10–1000	67
pDA/AuNPs/SPCE	ECS	2.0	10–500	This work

[a] AMTS: aminopropyltriethoxysilane; AuNPs: gold nanoparticles; CPE: carbon pencil electrode; CS: chitosan; CV: cyclic voltammetry; DPV: differential pulse voltammetry; *I–t* : amperometry; PEI: polyetherimide; LIG: laser-induced graphene; GCE: glassy carbon electrode; FTO: fluorine-doped tin oxide; GR: graphene.

Table 2 Determination of nitrite in processed meat (ham and salami) samples at PDA/AuNPs/SPCE

		Standard calibration			Standard additions		
Samples	D^a (μM)	A^b (μM)	F^c (μM)	% R^d	A (μM)	F (μM)	% R (±RSD)^e
Ham	3.96	10.0	3.1×10^2	2.2×10^4	10.0	13.13	94.0 ± 3
		25.0	1.0×10^5	3.6×10^5	25.0	30.05	103.9 ± 2
		50.0	4.4×10^5	8.2×10^5	50.0	54.58	101.1 ± 1
Salami	5.00	10.0	2.2×10^{11}	1.4×10^{12}	10.0	14.86	99.1 ± 3
		25.0	8.9×10^{11}	3.0×10^{12}	25.0	29.77	99.2 ± 5
		50.0	1.7×10^{12}	3.0×10^{12}	50.0	46.77	85.0 ± 7

^{a} D: detected using the current method. ^{b} A: Added. ^{c} F: Found. ^{d} R: recovery (% $R = 100 \times (F - A)/A$). ^{e} RSD of 3 measurements.

3.5. Real sample analysis

The practical applicability of the pDA/AuNPs-modified electrode was evaluated by testing its performance for nitrite determination in processed meat samples, specifically ham and salami obtained from a local market. The samples were spiked with three different concentrations of nitrite (10, 25 and 50 μM), and their capacitive responses were measured (Fig. 4A/B).

When comparing the relative capacitance obtained from the spiked meat samples with that of the buffer solutions using the standard calibration curve, a significant deviation in the recovery results was observed, indicating the presence of a large matrix effect in these processed meat samples (Table 2). It is worth mentioning that this the first report to address this matrix effect it in the analysis of food samples using capacitance spectroscopy.

To account for this matrix effect, the standard additions method was alternatively examined. However, as shown in Fig. 4C and S7,† the conventional standard additions plot was still non-linear, which was expected since the relative capacitance is proportional to the logarithm of the nitrite concentrations. As solution, the obtained standard additions plot was mathematically transformed or corrected by dividing the relative capacitance by the slope of the standard calibration curve (Fig. 4D and S8†). Subsequently, nitrite concentrations were determined with acceptable recovery percentages (Table 2), demonstrating that the standard additions method provides a more accurate measurement of nitrite concentrations in the analysed samples compared to using a standard curve. This finding confirms that the prepared sensor can be practically utilized for the detection of nitrite in real samples of processed meat and potentially in vegetables and fruits as well. Furthermore, as illustrated in Table 2, the relative standard deviation obtained from three different measurements ranged between 1% and 7%. This indicates that the sensor exhibits acceptable electrode-to-electrode reproducibility in the detection of nitrite in real samples.

4. Conclusion

In summary, the study successfully prepared a polydopamine/AuNPs-modified SPCE using electrodeposition methods. This approach offered a flexible, cost-effective technique for creating modified electrode surfaces that are controllable, uniform and reproducible. The redox properties of the polydopamine film were leveraged to achieve sensitive and selective detection of nitrite ions using electrochemical capacitance spectroscopy. Moreover, the developed sensor demonstrated the capability to detect low concentrations of nitrite ions in spiked buffer solutions and processed meat samples, despite the presence of a significant matrix effect. The current research presented a promising platform for the fabrication of capacitance-based sensors for anions, paving the way for future applications in the field.

Author contributions

F. K. A.: formal analysis, investigation, methodology, writing original draft, funding acquisition; A. R.: data, formal analysis, investigation, writing original draft; M. M.: formal analysis, investigation, writing original draft; S. B. A.: supervision, writing – review& editing; B. Y. A.: formal analysis, writing original draft; N. R.: conceptualization, funding acquisition, resources, supervision, writing – review & editing.

Conflicts of interest

The authors declare no conflict of interest.

Acknowledgements

The authors extend their appreciation to the Deanship of Scientific Research at Imam Mohammad Ibn Saud Islamic University (IMSIU) for funding and supporting this work through Research Partnership Program no. RP-21-09-69.

Notes and references

1 R. Cammack, C. L. Joannou, X.-Y. Cui, C. Torres Martinez, S. R. Maraj and M. N. Hughes, *Biochim. Biophys. Acta, Bioenerg.*, 1999, **1411**, 475–488.
2 M. Karwowska and A. Kononiuk, *Antioxidants*, 2020, **9**, 241.
3 M. Correia, Â. Barroso, M. F. Barroso, D. Soares, M. B. P. P. Oliveira and C. Delerue-Matos, *Food Chem.*, 2010, **120**, 960–966.
4 C. Menard, F. Heraud, J.-L. Volatier and J.-C. Leblanc, *Food Addit. Contam., Part A: Chem., Anal., Control, Exposure Risk Assess.*, 2008, **25**, 971–988.

5 S. Y. Choi, M. J. Chung, S.-J. Lee, J. H. Shin and N. J. Sung, *Food Control*, 2007, **18**, 485–491.
6 P. Santamaria, Nitrate in vegetables: toxicity, content, intake and EC regulation, *J. Sci. Food Agric.*, 2006, **86**, 1–10.
7 M. M. Pelletier, P. Kleinbongard, L. Ringwood, R. Hito, C. J. Hunter, A. N. Schechter, M. T. Gladwin and A. Dejam, *Free Radicals Biol. Med.*, 2006, **41**, 541–548.
8 J. Zhang, C. Yue, Y. Ke, H. Qu and L. Zeng, *Adv. Agrochem*, 2023, **2**(2), 127–141.
9 Y. Guo, R. Wang, C. Wei, Y. Li, T. Fang and T. Tao, *Food Chem.*, 2023, **415**, 135749.
10 M. Sepahvand, F. Ghasemi and H. M. Seyed Hosseini, *Food Chem. Toxicol.*, 2021, **149**, 112025.
11 C. T. K. Tran, H. T. T. Tran, H. T. T. Bui, T. Q. Dang and L. Q. Nguyen, *J. Sci.: Adv. Mater. Devices*, 2017, **2**, 172–177.
12 A. Rabti, S. Ben Aoun and N. Raouafi, *Microchim. Acta*, 2016, **183**, 3111–3117.
13 A. Diarisso, M. Fall and N. Raouafi, *Environ. Sci.: Water Res. Technol.*, 2018, **4**, 1024–1034.
14 M. L. Sall, B. Fall, I. Diédhiou, E. H. Dièye, M. Lo, A. K. D. Diaw, D. Gningue-Sall, N. Raouafi and M. Fall, *Chem. Afr.*, 2020, **3**, 499–512.
15 B. R. Kozub, N. V. Rees and R. G. Compton, *Sens. Actuators, B*, 2010, **143**, 539–546.
16 Z. Yang, X. Zhou, Y. Yin and W. Fang, *Anal. Lett.*, 2021, **54**, 2826–2850.
17 X. Li, J. Ping and Y. Ying, *TrAC, Trends Anal. Chem.*, 2019, **113**, 1–12.
18 A. Rhouati, M. Berkani, Y. Vasseghian and N. Golzadeh, *Chemosphere*, 2022, **291**, 132921.
19 P. R. Bueno, R. Hein, A. Santos and J. J. Davis, *Phys. Chem. Chem. Phys.*, 2020, **22**, 3770–3774.
20 S. Ben Aissa, A. Mars, G. Catanante, J.-L. Marty and N. Raouafi, *Talanta*, 2019, **195**, 525–532.
21 B. L. Garrote, A. Santos and P. R. Bueno, *Nat. Protoc.*, 2020, **15**, 3879–3893.
22 A. Raouafi, A. Rabti and N. Raouafi, *Microchim. Acta*, 2017, **184**, 4351–4357.
23 F. K. Algethami, A. Rabti, M. Mastouri, S. Ben Aoun, B. Y. Abdulkhair and N. Raouafi, *Talanta*, 2023, **258**, 124445.
24 F. C. B. Fernandes, J. R. Andrade and P. R. Bueno, *Sens. Actuators, B*, 2019, **291**, 493–501.
25 J. Piccoli, R. Hein, A. H. El-Sagheer, T. Brown, E. M. Cilli, P. R. Bueno and J. J. Davis, *Anal. Chem.*, 2018, **90**, 3005–3008.
26 M. Hamami, A. Mars and N. Raouafi, *Microchem. J.*, 2021, **165**, 106102.
27 M. Hamami, N. Raouafi and H. Korri-Youssoufi, *Appl. Sci.*, 2021, **11**, 1382.
28 R. M. B. Oliveira, F. C. B. Fernandes and P. R. Bueno, *Electrochim. Acta*, 2019, **306**, 175–184.
29 J. Szewczyk, D. Aguilar-Ferrer and E. Coy, *Eur. Polym. J.*, 2022, **174**, 111346.
30 R. Sanchis-Gual, M. Coronado-Puchau, T. Mallah and E. Coronado, *Coord. Chem. Rev.*, 2023, **480**, 215025.
31 N. Leibl, L. Duma, C. Gonzato and K. Haupt, *Bioelectrochemistry*, 2020, **135**, 107541.
32 Y. Lu, Y. Dong, X. Li and Q. He, *J. Food Sci.*, 2016, **81**, C2692–C2696.
33 J. Tian, S.-Y. Deng, D.-L. Li, D. Shan, W. He, X.-J. Zhang and Y. Shi, *Biosens. Bioelectron.*, 2013, **49**, 466–471.
34 F. Li, L. Yang, C. Zhao and Z. Du, *Anal. Methods*, 2011, **3**, 1601–1606.
35 A. Rabti, R. Zayani, M. Meftah, I. Salhi and N. Raouafi, *Microchim. Acta*, 2020, **187**, 1–9.
36 S. Daboss, J. Lin, M. Godejohann and C. Kranz, *Anal. Chem.*, 2020, **92**, 8404–8413.
37 B. L. Garrote, A. Santos and P. R. Bueno, *Nat. Protoc.*, 2020, **15**, 3879–3893.
38 G. Xu, J. Hou, Y. Zhao, J. Bao, M. Yang, H. Fa, Y. Yang, L. Li, D. Huo and C. Hou, *Sens. Actuators, B*, 2019, **287**, 428–436.
39 M. Amiri, E. Amali, A. Nematollahzadeh and H. Salehniya, *Sens. Actuators, B*, 2016, **228**, 53–58.
40 J. Lin, S. Daboss, D. Blaimer and C. Kranz, *Nanomaterials*, 2019, **9**, 242.
41 J. Kund, S. Daboss, T. M. D'Alvise, S. Harvey, C. V. Synatschke, T. Weil and C. Kranz, *Nanomaterials*, 2021, **11**, 1964.
42 P. Kanyong, S. Rawlinson and J. Davis, *Sens. Actuators, B*, 2016, **233**, 528–534.
43 E. Laviron, *J. Electroanal. Chem. Interfacial Electrochem.*, 1979, **100**, 263–270.
44 A. Hammami, J. Kuliček and N. Raouafi, *Food Chem.*, 2016, **209**, 274–278.
45 D. R. Kumar, S. Kesavan, T. T. Nguyen, J. Hwang, C. Lamiel and J.-J. Shim, *Sens. Actuators, B*, 2017, **240**, 818–828.
46 E. Laviron, *J. Electroanal. Chem. Interfacial Electrochem.*, 1979, **101**, 19–28.
47 P. R. Bueno, G. Mizzon and J. J. Davis, *J. Phys. Chem. B*, 2012, **116**, 8822–8829.
48 C. Lete, M. Chelu, M. Marin, S. Mihaiu, S. Preda, M. Anastasescu, J. M. Calderón-Moreno, S. Dinulescu, C. Moldovan and M. Gartner, *Sens. Actuators, B*, 2020, **316**, 128102.
49 A. Adiraju, R. Munjal, C. Viehweger, A. Al-Hamry, A. Brahem, J. Hussain, S. Kommisetty, A. Jalasutram, C. Tegenkamp and O. Kanoun, *Sensors*, 2023, **23**, 2961.
50 D. Gobelli, N. Mariano Correa, M. Fátima Barroso, F. Moyano and P. G. Molina, *Electroanalysis*, 2015, **27**, 1883–1891.
51 G. Maduraiveeran and R. Ramaraj, *J. Anal. Sci. Technol.*, 2017, **8**, 14.
52 M. Talbi, A. Al-Hamry, P. R. Teixeira, A. Bouhamed, S. Azzouzi, L. G. Paterno, M. B. Ali and O. Kanoun, in *2019 16th International Multi-Conference on Systems, Signals & Devices (SSD)*, 2019, pp. 1–4.
53 S. Nasraoui, A. Al-Hamry, P. R. Teixeira, S. Ameur, L. G. Paterno, M. Ben Ali and O. Kanoun, *J. Electroanal. Chem.*, 2021, **880**, 114893.
54 R. Mo, X. Wang, Q. Yuan, X. Yan, T. Su, Y. Feng, L. Lv, C. Zhou, P. Hong, S. Sun, Z. Wang and C. Li, *Sensors*, 2018, **18**, 1986.
55 A. L. Lavanya, K. G. B. Kumari, K. R. S. Prasad and P. K. Brahman, *Electroanalysis*, 2021, **33**, 1096–1106.

56 S. H. Mohd Taib, K. Shameli, P. Moozarm Nia, M. Etesami, M. Miyake, R. Rasit Ali, E. Abouzari-Lotf and Z. Izadiyan, *J. Taiwan Inst. Chem. Eng.*, 2019, **95**, 616–626.
57 M. Zhang, F. Cheng and F. Gan, *Int. J. Electrochem. Sci.*, 2015, **10**, 5905–5913.
58 P. Saha, R. Akter, S. Shaheen Shah, W. Mahfoz, Md. A. Aziz and A. J. Saleh Ahammad, *Chem.–Asian J.*, 2022, **17**, e202200823.
59 D. W. Scott and Y. Alseiha, *J. Anal. Sci. Technol.*, 2017, **8**, 17.
60 M. Braik, C. Dridi, A. Ali, M. N. Abbas, M. Ben Ali and A. Errachid, *Org. Electron.*, 2015, **16**, 77–86.
61 S. C. Patrick, R. Hein, P. D. Beer and J. J. Davis, *J. Am. Chem. Soc.*, 2021, **143**, 19199–19206.
62 M. Etesami, N. Chandran, M. H. Hussin, A. Ripin, R. Adnan, A. N. Ahmad Sujari and N. Mohamed, *Int. J. Electrochem. Sci.*, 2016, **11**, 8332–8345.
63 Y. Zhang, F. Wen, J. Tan, C. Jiang, M. Zhu, Y. Chen and H. Wang, *J. Electroanal. Chem.*, 2017, **786**, 43–49.
64 H. Huang, Y. Yue, L. Li and J.-J. Zhu, *J. Electrochem. Soc.*, 2017, **164**, H321.
65 C. Li, D. Chen, Y. Wang, X. Lai, J. Peng, X. Wang, K. Zhang and Y. Cao, *Sensors*, 2019, **19**, 1304.
66 Y. Han, R. Zhang, C. Dong, F. Cheng and Y. Guo, *Biosens. Bioelectron.*, 2019, **142**, 111529.
67 Y.-M. Zhang, H.-P. Huang and L. Xu, *Chin. J. Anal. Chem.*, 2020, **48**, e20032–e20037.